Journal of Molecular Catalysis A: Chemical 344 (2011) 53–61

Contents lists available at ScienceDirect

Journal of Molecular Catalysis A: Chemical

journal homepage: www.elsevier.com/locate/molcata

Role of CO_2 in ethylbenzene dehydrogenation over Fe_2O_3(0 0 0 1) from first principles

Xiao-Xiang He [a], Chen Fan [a], Xiong-Yi Gu [a,*], Xing-Gui Zhou [a], De Chen [b], Yi-An Zhu [a,*]

[a] State Key Laboratory of Chemical Engineering, East China University of Science and Technology (ECUST), Shanghai 200237, China
[b] Department of Chemical Engineering, Norwegian University of Science and Technology (NTNU), N-7491 Trondheim, Norway

ARTICLE INFO

Article history:
Received 12 February 2011
Received in revised form 28 April 2011
Accepted 1 May 2011
Available online 7 May 2011

Keywords:
DFT
Ethylbenzene dehydrogenation
CO_2
Fe_2O_3(0 0 0 1)

ABSTRACT

First-principles calculations based on density functional theory have been performed to elucidate the reaction mechanism for ethylbenzene dehydrogenation and the role of CO_2 in H removal. On the basis of the experimental information and theoretical prediction, three model surfaces with Fe-, ferryl- and O-termination are constructed to represent the active Fe_2O_3(0 0 0 1) surface. The calculated results indicate that on all of the three surfaces the C–H activation in the methylene group followed by the dehydrogenation of the methyl group is kinetically more favorable. The energy barriers for ethylbenzene dehydrogenation are lowest on the O-terminated surface, but the generated styrene is adsorbed too strongly to be released. As CO_2 decomposition and the formation of HCOO are hindered by the relatively high activation energies, CO_2 cannot serve as the oxidant to recover the O- and ferryl-terminated surfaces to keep the redox cycle. At the steady state of the reaction the coupling mechanism dominates on the Fe-terminated surface, with the synergistic effect between ethylbenzene dehydrogenation and the reverse water–gas shift reaction. Since the energy barrier for the formation of COOH is comparable to that for H_2 formation, both the one-step and two-step pathways are predicted to contribute to the coupling mechanism, although the former is more probable.

1. Introduction

The dehydrogenation of ethylbenzene to produce styrene is an important industrial process, which is carried out over iron oxide-based catalyst at temperatures around 870 K in the presence of steam. As this commercial process consumes a large amount of energy, CO_2 is recently used instead as the co-feed gas, which is believed to be energy-saving and environmentally friendly. Furthermore, through the coupling of ethylbenzene dehydrogenation with the reverse water–gas shift reaction, the ethylbenzene conversion can be significantly improved, arising from the simultaneous hydrogen elimination [1–4].

Two mechanisms, namely the coupling mechanism and the redox cycle mechanism, are traditionally proposed for ethylbenzene dehydrogenation in the presence of CO_2, as illustrated in Fig. 1. In the coupling mechanism, the generated H atoms through the dehydrogenation of ethylbenzene react with CO_2 to produce OH, COOH or HCOO which further combines with H to form H_2O. Alternatively, the detached H atoms first combine to produce H_2, and then H_2 is dissociated to yield H atoms for the subsequent reverse water–gas shift reaction. These two pathways are generally called one-step and two-step pathways [5,6].

In the redox cycle mechanism, the H atoms in ethylbenzene are abstracted by lattice O atoms to form H_2O, leading to the reduction of catalyst surfaces. Then CO_2 is decomposed to compensate for surface O to keep the catalyst activity and achieve the reaction cycle.

Some experimental efforts have been devoted to interpreting the mechanism for this coupling system. Badstube et al. [7] investigated the dehydrogenation of ethylbenzene over iron oxide catalyst supported on activated carbon in the presence of CO_2. Apart from styrene, benzene, and toluene, CO and H_2O were captured with the constant molar ratio of 0.8 during the process. Comparing the experimental data to the postulated mechanisms, they believed that both the reverse water–gas shift reaction and the redox cycle mechanism make contributions to ethylbenzene dehydrogenation. Likewise, Chang et al. [8] examined the beneficial effect of CO_2 on the dehydrogenation of ethylbenzene to styrene over zeolite-supported iron oxide catalyst. Styrene, H_2O, CO, and a small amount of H_2 were produced. As shown in Fig. 1, the coupling mechanism succeeds in accounting for the formation of H_2 while the detected CO and H_2O may be yielded either through the decomposition of CO_2 followed by H abstraction from ethylbenzene by surface O or via the reverse water–gas shift reaction. Hence, they proposed that both the coupling and redox cycle mechanisms are probable.

* Corresponding authors. Tel.: +86 21 64253072; fax: +86 21 64253528.
E-mail addresses: gxiongy@ecust.edu.cn (X.-Y. Gu), yanzhu@ecust.edu.cn (Y.-A. Zhu).

1381-1169/$ – see front matter © 2011 Elsevier B.V. All rights reserved.
doi:10.1016/j.molcata.2011.05.002

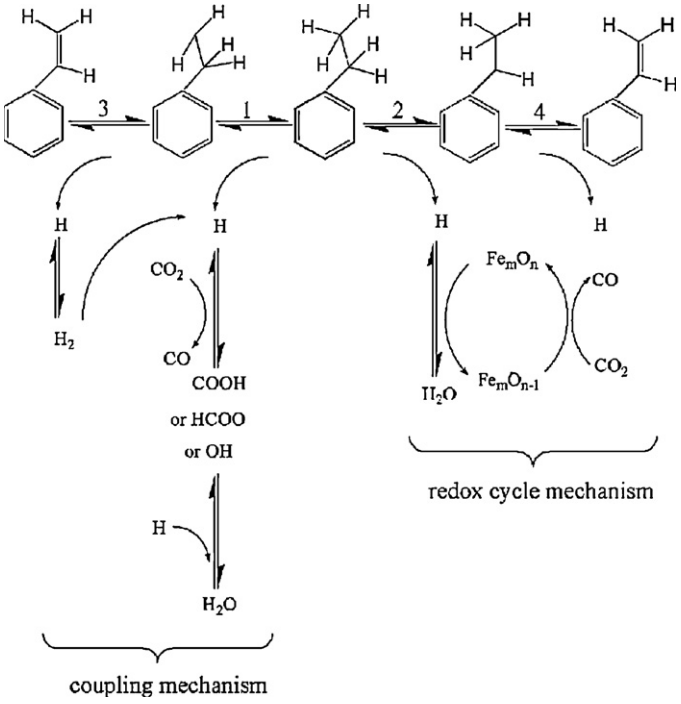

Fig. 1. Two reaction mechanisms for ethylbenzene dehydrogenation in the presence of CO_2.

However, some groups suggested that only one of the two mechanisms is dominant in this process. Sun et al. [9] have examined the dehydrogenation of ethylbenzene over a series of Fe and V supported catalysts in the presence of CO_2 by means of temperature-programmed desorption. The experimental data indicated that the ethylbenzene conversion is associated with the conversion of CO_2, and that there exists a synergistic effect between ethylbenzene dehydrogenation and the reverse water–gas shift reaction. In addition, CO_2 was considered to be activated through either basic or redox sites, and both the one-step and the two-step pathways were proposed. In contrast, Sugino et al. [2] investigated ethylbenzene dehydrogenation over activated carbon-supported iron oxide catalyst by X-ray diffraction analysis. They found the amounts of CO and H_2O produced during the reaction agree well with the amount of styrene, indicating a redox cycle as follows: (1) lattice O atoms abstract H from ethylbenzene to give styrene; (2) CO_2 oxidizes O defects in the iron oxide phase.

Thus, while many attempts have been made to elucidate the mechanism for ethylbenzene dehydrogenation in the presence of CO_2, the way how CO_2 is activated and the role of CO_2 activation in H removal are still under debate.

On the other hand, the active centers for ethylbenzene dehydrogenation and CO_2 activation remain elusive as well. Iron oxide catalyst has been extensively applied in the dehydrogenation of ethylbenzene, which shows an excellent performance [5–7,10–15]. Zhu et al. [16] has investigated the dehydrogenation of ethylbenzene over potassium-promoted iron oxide-based catalyst with high time resolution using on-line mass spectroscopy, and claimed that the fully oxidized iron phases containing only Fe^{3+} ions are responsible for the high catalytic activity. However, Kuhrs et al. [17] suggested that while Fe_3O_4 is inactive towards this reaction, an induction period is necessary before Fe_2O_3 becomes active. Similarly, Weiss et al. [18–20] investigated ethylbenzene dehydrogenation over single-crystalline iron oxide model catalyst films grown epitaxially onto Pt(1 1 1) substrates. It was found that atomic surface defects act as the active centers, whereas Fe_3O_4(1 1 1) is always inactive.

In this contribution, first-principles calculations based on density functional theory (DFT) are performed to explore ethylbenzene dehydrogenation in the presence of CO_2 on the Fe-, ferryl- and O-terminated Fe_2O_3(0 0 0 1) surfaces. Firstly, on the basis of the experimental information, three models are constructed for the three surfaces. Secondly, the adsorption energies of the reaction intermediates and the activation energies for the elementary steps involved are calculated to elucidate the dominant active surface and reaction pathway. Finally, we conclude by discussing the implication of our results for understanding the reaction mechanism for ethylbenzene dehydrogenation and the key role of CO_2 in H removal.

2. Computational details

The first-principles calculations have been performed by the VASP code [21–23]. The generalized gradient approximation functional proposed by Perdew et al. was used [24]. The interactions between valence electrons and ion cores are represented by Blöchl's all-electron-like projector augmented wave method (PAW) [25], which regards the d7s1 states as the valence configuration for Fe, s2p4 for O and s2p2 for C. A plane wave energy cutoff of 400 eV was used in the present calculations. Geometries were relaxed using the conjugate gradient algorithm [26] until the forces on all the unconstrained atoms are less than 0.03 eV/Å. There is a magnetic element (Fe) involved in the system, and therefore spin-polarized effect has been considered. The calculations performed by Bergermayer [27] showed that surface magnetism plays a key role in the quantitative description of total energy.

α-Fe_2O_3 has a hexagonal close-packed structure of slightly distorted O, with 2/3 of the interstitial octahedral sites being occupied by Fe ions [28]. It is very stable and often the end form of the transformation of other iron oxides. DFT calculations have been previously carried out to explore the geometry of α-Fe_2O_3 [29,30], and through the surface energy calculations it was found that the (0 0 0 1) surface is most stable [19].

Starting from bulk α-Fe_2O_3, several terminations are possible to derive the (0 0 0 1) surfaces. The previous theoretical work indicated that at low O chemical potential (i.e., low O_2 partial pressure or high temperature), the Fe-terminated surface shown in Fig. 2(a) is found to be the most stable surface, whereas at high O chemical potential the (0 0 0 1) surface of hematite is completely covered with O atoms [the O-terminated surface shown in Fig. 2(b)] [27,31–33].

Experimentally, the (0 0 0 1) surface has been characterized in detail under ultra high vacuum, indicating that both the Fe- and O-termination can be observed with a somewhat complex mixture of surface phases existing under different temperatures and O_2 partial pressures [34,35]. On the other hand, Chambers et al. [36] investigated the termination of the epitaxial α-Fe_2O_3(0 0 0 1) prepared by oxygen–plasma-assisted molecular beam, and claimed that despite the highly oxidizing conditions the Fe-terminated surface is most stable.

Besides, a ferryl (Fe=O) termination which can be regarded as one special type of defects was proposed [37–39], as represented schematically in Fig. 2(c). Ferryl species are predicted to be active in the selective oxidation and dehydrogenation reactions, and coexist with the domains of Fe-termination at certain O_2 pressures. Bergermayer et al. [27] claimed that the Fe-terminated surface has the ability to accept and release O under the thermodynamic conditions applied in the catalytic oxidation of ethylbenzene, and the shuttling between the Fe-termination (Fe–O3–Fe) and the ferryl-termination (O–Fe–O3–Fe) may play a key role in the reaction mechanism.

As a result, these three surfaces are singled out to investigate the dehydrogenation of ethylbenzene in the presence of CO_2. A

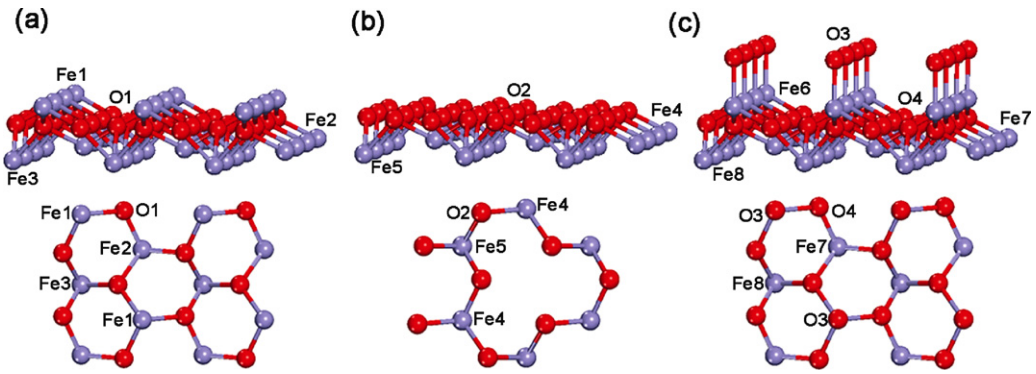

Fig. 2. Geometries of Fe_2O_3(0 0 0 1) with (a) the Fe-termination, (b) the O-termination, and (c) the ferryl-termination. Fe atoms are colored blue, and O atoms are colored red.

slab model with nine layers (ten layers for ferryl-termination) was used to achieve a good balance between the computational cost and accuracy. The vacuum gap between two-dimensional periodic slabs was set as large as 10 Å. A $p(2 \times 2)$ supercell and a $2 \times 2 \times 1$ k-point mesh were used. For the Fe-termination and ferryl-termination, the bottom five layers were fixed, and the top four or five layers as well as the adsorbates were allowed to relax. For the O-termination, the bottom six layers were fixed, and the top three layers as well as the adsorbates were relaxed.

As proposed previously, the DFT–GGA level is adequate to give the reasonable bond distances and magnetic ordering in bulk iron oxide [27], and therefore it is reasonable to expect that this level of theory may also give meaningful geometric and energetic properties for the surfaces of iron oxide. Thus, LDA + U which is only important in the calculations such as photoemission spectra and pressure-induced metal–insulator phase transitions of Fe_2O_3 has not been considered in the present work.

The adsorption energy in this work is defined as

$$\Delta E_{ads} = E_{adsorbate+sur} - E_{adsorbate} - E_{sur} \quad (1)$$

where $E_{adsorbate+sur}$ is the total energy of the Fe_2O_3(0 0 0 1) surface with the adsorbate adsorbed, $E_{adsorbate}$ the total energy of an isolated adsorbate, and E_{sur} the total energy of the bare Fe_2O_3(0 0 0 1) surface. A negative ΔE_{ads} indicates the adsorption is exothermic.

The dimer method [40] was used to locate transition states, in which the saddle point is optimized using a force-based conjugate-gradient method [26] until the maximum force in every degree of freedom is less than 0.03 eV/Å. The Hessian matrix for the potential energy surface was then calculated using finite difference approximation and diagonalized to find the normal modes of the transition state. The adsorbates and the surface atoms to which the adsorbates are attached were displaced in the direction of each Cartesian coordinate while the other surface atoms were kept rigid during these finite difference calculations. All the transition states have been verified with only one imaginary vibrational frequency, and the calculated data can be found in Supplementary Material (see Table S1).

3. Results and discussion

3.1. Adsorption of ethylbenzene, phenylethyl and styrene

3.1.1. Ethylbenzene adsorption

The molecular adsorption of ethylbenzene on the Fe-, ferryl-, and O-terminated surfaces was first investigated. Geometry optimization has been performed with the phenyl ring of ethylbenzene initially parallel to the surfaces. It was found that the ethylbenzene molecule is repelled upwards, drifting over all the three surfaces. The most stable adsorption configurations and the corresponding adsorption energies of ethylbenzene are given in Fig. 3(a)–(c) and Table 1, respectively.

In the energetically favorable adsorption configuration of ethylbenzene on the Fe-terminated surface, the ortho-carbon atom of the phenyl ring points towards the Fe surface atom, with the Fe–C distance of 2.38 Å. Because of the formation of the C–Fe bond, the geometry of the molecule is slightly tilted, and the corresponding adsorption energy is highest among the three surfaces.

On the ferryl-terminated surface, the most stable adsorption configuration of ethylbenzene is found to be located among surface O atoms, as shown in Fig. 3(b), indicating that the surface O atoms are unfavorable for ethylbenzene to be adsorbed. In contrast, the variation in the ethylbenzene adsorption energies at the different sites of the O-terminated surface is negligible. However, the highest adsorption energy on the O-terminated surface is found to be equal to that on the ferryl-terminated surface (see Table 1). The less stable adsorption configurations of ethylbenzene on the three surfaces and the corresponding adsorption energies are given in Supplementary Material (Figs. S1–S3 and Tables S2–S4).

Comparing the adsorption energies of ethylbenzene on the three surfaces, one can see that the binding on the Fe-terminated surface is much stronger than those on the ferryl- and O-terminated surfaces, indicating that the Fe surface atoms play a key role in ethylbenzene adsorption. This is supported by the previous experiments [19,41] that the chemisorbed ethylbenzene was captured on the Fe-terminated α-Fe_2O_3(0 0 0 1) or Fe_3O_4(1 1 1) surface, while on the O-terminated FeO(1 1 1) surface only the physisorption and condensation of ethylbenzene were observed. This is because on the Fe-terminated surface, ethylbenzene is chemisorbed via rather a strong interaction between the phenyl ring π-electron system and the acidic Fe surface atoms [20].

On the other hand, the experimentally determined adsorption energy (0.66 eV) [17,41] is much higher than our calculated values. Two possible reasons are responsible for this discrepancy. Firstly, the GGA functional in DFT describes the electrostatic interaction part of van der Waals interaction, which generally underestimates the strength of physisorption. Secondly, the realistic surface is far more complex and includes a large number of surface defects that perhaps are favorable for ethylbenzene adsorption.

Table 1
The adsorption energies for ethylbenzene, intermediates and styrene on the three surfaces.

Species	E_{ads} (eV)		
	Fe-terminated	Ferryl-terminated	O-Terminated
Ethylbenzene	−0.33	−0.11	−0.11
1-Phenylethyl	−1.71	−2.31	−2.76
2-Phenylethyl	−1.25	−1.63	−1.86
Styrene	−0.87	−0.70	−1.92

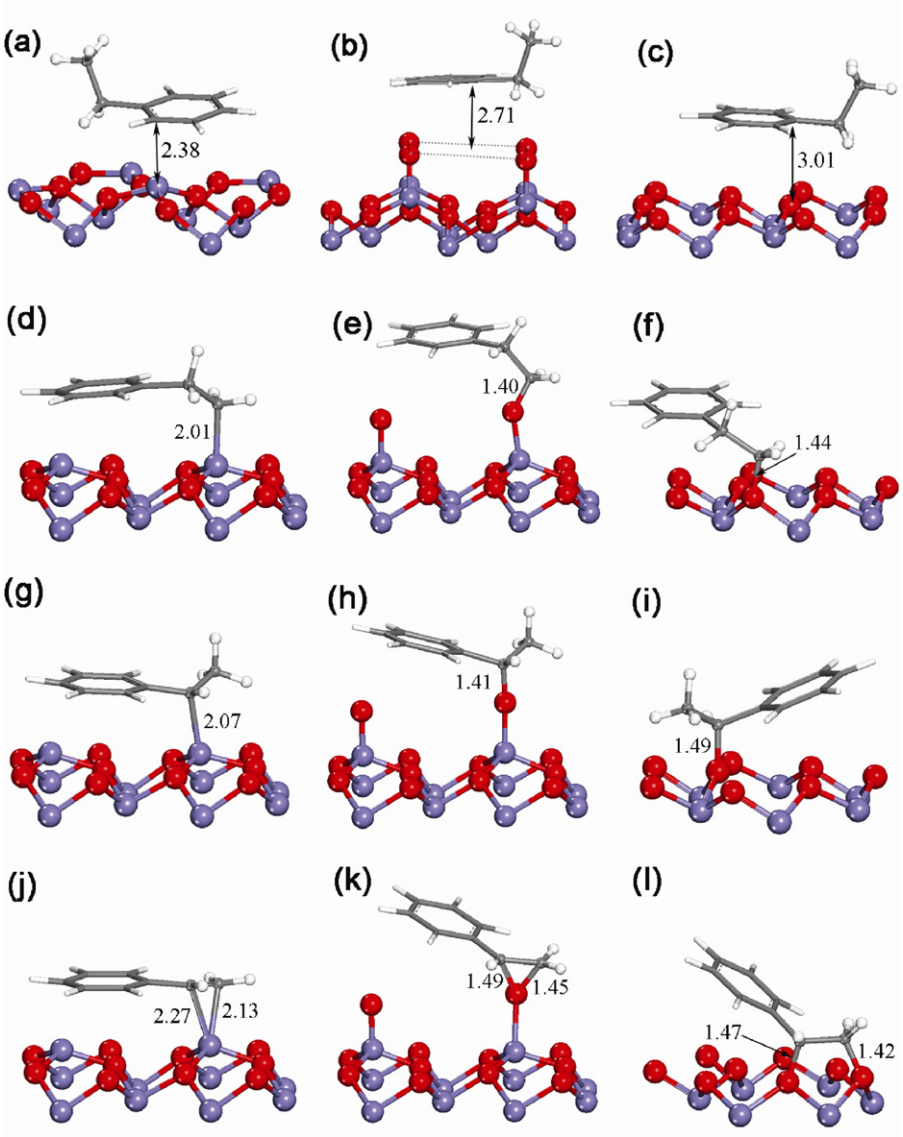

Fig. 3. Adsorption configurations of ethylbenzene, 1-phenylethyl, 2-phenylethyl, and styrene (a), (d), (g), (j) on the Fe-terminated surface, (b), (e), (h), (k) on the ferryl-terminated surface, and (c), (f), (i), (l) on the O-terminated surface.

3.1.2. 1-Phenylethyl ($C_6H_5CH_2CH_2$) and 2-phenylethyl ($C_6H_5CHCH_3$) adsorption

The 1-phenylethyl and 2-phenylethyl species are two possible reaction intermediates in ethylbenzene dehydrogenation. Both the $–CH_2$ fragment in 1-phenylethyl and the –CH– fragment in 2-phenylethyl have one unpaired electron, and can be readily adsorbed on the surfaces. For each species, several adsorption configurations with different binding sites and orientations of the phenyl ring have been considered (see Figs. S4–S9 and Tables S5–S10 in Supplementary Material). The most stable adsorption configurations on the three surfaces are shown in Fig. 3(d)–(i), and the corresponding adsorption energies are given Table 1.

From Fig. 3(d)–(i), one can see that on the Fe-terminated surface the 1-phenylethyl and 2-phenylethyl species bind to surface Fe atoms, while on the ferryl- and O-terminated surfaces the lattice O atoms act as the active sites for adsorption. On the other hand, the phenyl ring is positioned parallel to the Fe-terminated surface whereas on the other two surfaces the phenyl ring is repelled towards vacuum, arising from the sterically hindered O atoms in the vicinity. With the comparison of the adsorption energies of 1- or 2-phenylethyl over the three surfaces, it is found that the O-terminated surface is most favorable for both 1- and 2-phenylethyl adsorption.

3.1.3. Styrene adsorption

Styrene is the target product in ethylbenzene dehydrogenation. The most stable adsorption configurations on the three surfaces are shown in Fig. 3(j)–(l), and the corresponding adsorption energies are given in Table 1. As the vinyl group has a half-saturated double bond (C=C), styrene can be adsorbed via the so-called π or di-σ mode. As shown in Fig. 3(j) and (k), vinyl binds to a surface Fe and O atom via the π adsorption mode on the Fe- and ferryl-terminated surfaces, respectively, while the interaction between styrene and the O-terminated surface is quite strong. In the most stable adsorption configuration [Fig. 3(l)], the two carbon atoms of vinyl bind to two lattice O atoms via the di-σ adsorption mode. The less stable adsorption configurations of styrene on the three surfaces and the corresponding adsorption energies are given in Supplementary Material (Figs. S10–S12 and Tables S11–S13).

From Table 1, one can see that the interaction strength between styrene and catalyst surface decreases from the O- to Fe-, and

further to ferryl-terminated surface. It was reported that the experimentally measured adsorption energy of styrene on the $Fe_2O_3(0001)$ surface was ~0.76 eV [17,41]. It is therefore reasonable to expect that the Fe- and ferryl-terminated surfaces are dominant under realistic experimental conditions. Moreover, the bonding of styrene on the Fe-terminated surface is stronger than that on the ferryl-terminated surface, merely because the unsaturated C=C bond with a polarizable π-electron orbital couples to the empty Fe 3d orbital.

3.2. Ethylbenzene dehydrogenation on the Fe-terminated surface

3.2.1. C–H bond activation

The cleavage of the C–H bond in ethylbenzene can take place in either the methyl or methylene group, and the respective products are the 1-phenylethyl and 2-phenylethyl species. Thus, two dehydrogenation pathways are shown in Fig. 1: ethylbenzene $\xrightarrow{1}$ 1-phenylethyl $\xrightarrow{3}$ styrene [denoted as PATH(I)] and ethylbenzene $\xrightarrow{2}$ 2-phenylethyl $\xrightarrow{4}$ styrene [denoted as PATH(II)], where the superscripts are the sequence numbers of the dehydrogenation elementary steps.

There are two ways for the first C–H bond-breaking in ethylbenzene on the Fe-terminated surface. One is the homolytic cleavage that usually takes place at the surface O sites. The other is the heterolytic splitting that is usually present on the surface with strong acid–base pairs involved. As the approach of ethylbenzene to surface O is blocked by the Fe atom positioned between them, the possibility of the homolytic cleavage of the C–H bond is disregarded on the Fe-terminated surface, and therefore the heterolytic cleavage is focused in the following section.

The potential energy diagrams and the transition states for PATH(I) are shown in Fig. 4. For the step 1, the C–H bond activation in the methyl fragment is 0.13 eV endothermic with the energy barrier of 1.01 eV. Here the activation energy for the step 1 is measured as the energy difference between the activated complex and the gaseous ethylbenzene molecule on the bare Fe-terminated surface because the interaction between ethylbenzene and iron oxide catalyst is rather weak and for the weakly adsorbed species such as CH_4, the energy barrier for the first dehydrogenation step is routinely defined with respect to the gaseous reactant. At the saddle point (TS1 in Fig. 4), the activated H does not move directly to the O site. Instead, it diffuses to the bridge site between the Fe and O surface atoms by elongating the C–H bond from 1.10 to 1.54 Å. The remaining 1-phenylethyl species is located at the Fe site for the subsequent dehydrogenation along the step 3. As for the step 3, the reaction heat and the activation energy are calculated to be −0.34 and 0.93 eV, respectively. At the saddle point (TS3), the C–H bond is stretched to 1.38 Å while the geometry of the remaining styrene resembles the adsorption configuration of isolated styrene, indicating the transition state is "late". One can see that the Fe surface atom plays a key role in the dehydrogenation of ethylbenzene on the Fe-terminated surface and serves as the active center. Finally, the energy barrier for styrene desorption is calculated to be 0.87 eV, which is moderate under the industrially applied temperature.

Along PATH(II), the energy barrier for the step 2 is 0.88 eV, lower than that for the step 1. Moreover, in contrast to the step 1, the step 2 is exothermic by 0.11 eV. Hence, the activation of the C–H bond in the methylene group is both kinetically and thermodynamically more favorable. For the subsequent dehydrogenation (the step 4), the energy barrier is calculated to be 1.08 eV and the process is 0.10 eV exothermic. Comparing the energy profiles for PATH(I) and PATH(II) shown in Fig. 4, one can see that the C–H activation in the methylene group followed by the dehydrogenation of the methyl group, namely PATH(II), is kinetically more favorable.

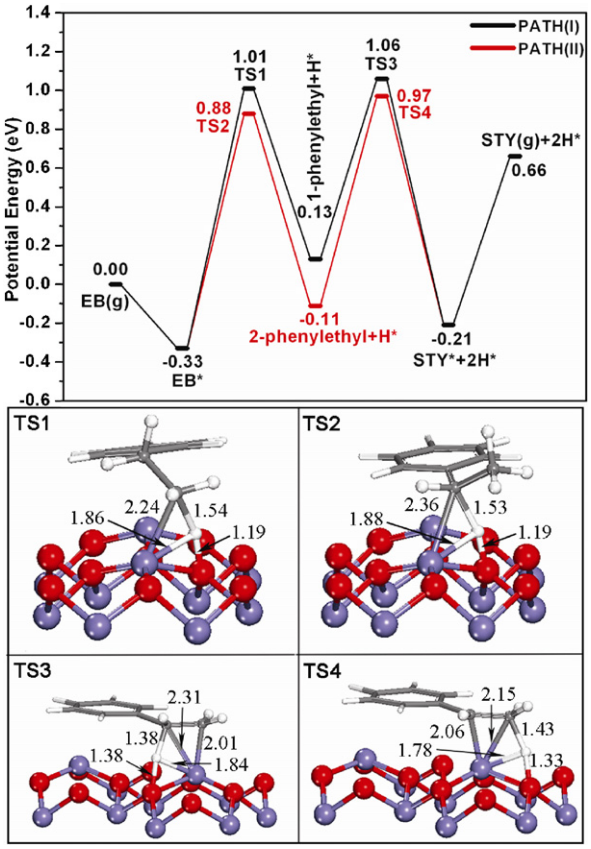

Fig. 4. Potential energy diagrams and transition states for ethylbenzene dehydrogenation on the Fe-terminated surface.

3.2.2. H_2 formation

The H atoms abstracted from ethylbenzene can be removed with the formation of H_2. The energy profile and the transition state (TS5) for H_2 formation on the Fe-terminated surface are shown in Fig. 5. In the initial state, two H atoms are adsorbed on the top of a Fe and O surface atom. As the reaction proceeds, the H atom of the OH group bridges the surface Fe and O atoms, with the length of the formed H–H bond of 1.11 Å. The energy barrier for this elementary step is calculated to be 1.49 eV, and the reaction is endothermic by 0.72 eV. Eventually, the generated H_2 desorbs from the surface with an energy barrier of 0.18 eV.

Moreover, the possibility of H_2 formation starting from the OH–OH configuration where two H atoms are adsorbed on the

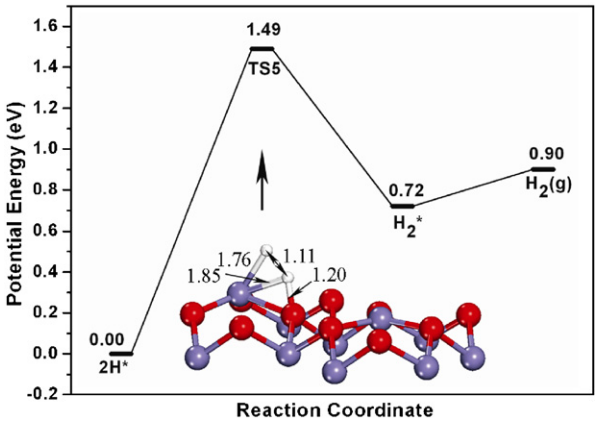

Fig. 5. Potential energy diagram and transition state for H_2 formation on the Fe-terminated surface.

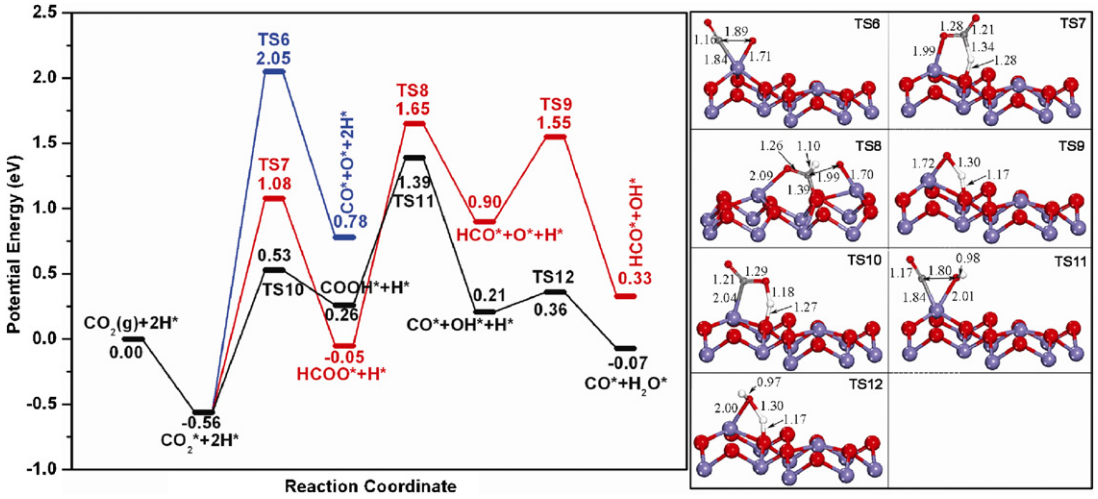

Fig. 6. Potential energy diagrams and transition states for three reaction pathways of CO_2 consumption on the Fe-terminated surface.

top of two surface O atoms was also examined, and the calculated energy barrier is as high as 2.77 eV, indicating that this pathway is kinetically hindered.

3.2.3. CO_2 consumption

It was reported that CO_2 is likely to promote H removal in ethylbenzene dehydrogenation [42]. On the Fe-terminated surface, the Fe surface atoms can provide reduction potential for CO_2 to be decomposed. For example, CO_2 molecule perhaps dissociates into CO and O, leading to the partial oxidization of the Fe-terminated surface or to the binding of O with H. Besides, CO_2 may react with H to produce COOH or HCOO, which can further combine with H to produce H_2O following the reverse water–gas shift reaction. Thus, these three reaction pathways were predicted to contribute to CO_2 consumption, and the adsorption configurations and energies of the species involved are given in Supplementary Material (Figs. S13–S22 and Tables S14–S23).

As shown in Fig. 6, the decomposition of CO_2 on the Fe-terminated surface is hindered by a high energy barrier of 2.05 eV. In the transition state (TS6 in Fig. 6), the C–O bond is elongated from 1.17 to 1.89 Å, with the CO and O species jointly adsorbed at the Fe site. Once one of the C–O bonds is broken, the energy barrier for CO desorption is calculated to be 0.98 eV.

The transition state for the formation of the formate species (HCOO) is shown in TS7 of Fig. 6. The H–O bond is stretched to 1.28 Å and the newly formed C–H bond is measured to be 1.34 Å. The energy barrier for the formation of HCOO is calculated to be 1.08 eV, and the activation energy for the subsequent decomposition of HCOO to produce HCO and O is 1.70 eV, with the transition state shown in TS8 of Fig. 6. Then it follows that the O atom combines with H to form OH (TS9 in Fig. 6), corresponding to an energy barrier of 0.65 eV. Alternatively, the O atom can oxidize the Fe-terminated surface. The overall energy barrier for this pathway ($CO_2 + 2H \rightarrow HCOO + H \rightarrow HCO + O + H \rightarrow HCO + OH$) is found to be 1.65 eV, as shown in Fig. 6.

As for the formation of the carboxyl species (COOH), the corresponding transition state is given in TS10 of Fig. 6, where the H–O bond is stretched to 1.27 Å and the formed O–H bond is measured to be 1.18 Å. The energy barrier for the formation of COOH is calculated to be 0.53 eV, much lower than that for the formation of HCOO. The COOH radical is further decomposed into CO and OH (TS11 in Fig. 6), and then the OH radical reacts with H to produce H_2O (TS12 in Fig. 6), with the energy barriers of 1.13 and 0.15 eV, respectively. With the comparison of the potential energy diagrams in Fig. 6, it is reasonable to expect that this reaction pathway ($CO_2 + 2H \rightarrow COOH + H \rightarrow CO + OH + H \rightarrow CO + H_2O$) is dominant for CO_2 consumption on the Fe-terminated surface, arising from the lowest overall energy barrier of 1.39 eV. Moreover, the O compensation through the decomposition of CO_2 and the formation of HCOO is predicted to be rather difficult.

Comparing the energy barrier for the third reaction pathway to activate CO_2 with that for H_2 formation, one can see that the presence of CO_2 benefits the removal of detached H atoms through the formation of H_2O. However, as there are always inherent limitations in DFT calculations and uncertainties of about 0.1 eV exist in DFT calculated activation energies, the consumption of atomic H through H_2 formation cannot be ruled out for their comparable energy barriers. Furthermore, Huang et al. [43,44] claimed that the O vacancies, and hence the reduced iron, can promote the formation of H_2.

As previously proposed, CO_2 could either react with the H atoms detached from ethylbenzene molecules or combine with the H atoms derived through the dissociation of molecular H_2, corresponding to the one-step and two-step pathway [5,6]. On the Fe-terminated surface, the formation of COOH is kinetically more favorable than H_2 formation, and therefore the one-step pathway plays a dominant role in the removal of H, though the two-step pathways are likely to coexist under realistic experimental conditions.

3.3. Oxidative dehydrogenation of ethylbenzene on the ferryl-terminated surface

3.3.1. C–H bond activation

The ferryl-termination is actually a type of defects on $Fe_2O_3(0\,0\,0\,1)$, which can be obtained by oxidizing the Fe-terminated surface. Its geometry resembles that of the oxides (such as Cr_2O_3 and V_2O_3) with the corundum structure, which is terminated by the active M=O (M = Cr, V, etc.) species [45,46]. On the basis of the aforementioned calculations, the ferryl-terminated surface is hard to be constructed through the oxidation of the Fe-terminated surface by CO_2. However, it can be attained during the catalyst preparation or through the oxidation by O_2 [27].

The potential energy diagrams and the geometries of the transition states for PATH(I) and PATH(II) on the ferryl-terminated surface are given in Fig. 7. The geometries of the transition states indicate that unlike the catalytic behavior of the Fe-terminated surface, H is attacked by a lattice O atom following the Mars van Krevelen mechanism [47] instead on the ferryl-terminated surface. From a thermodynamic point of view, the oxidative dehydrogena-

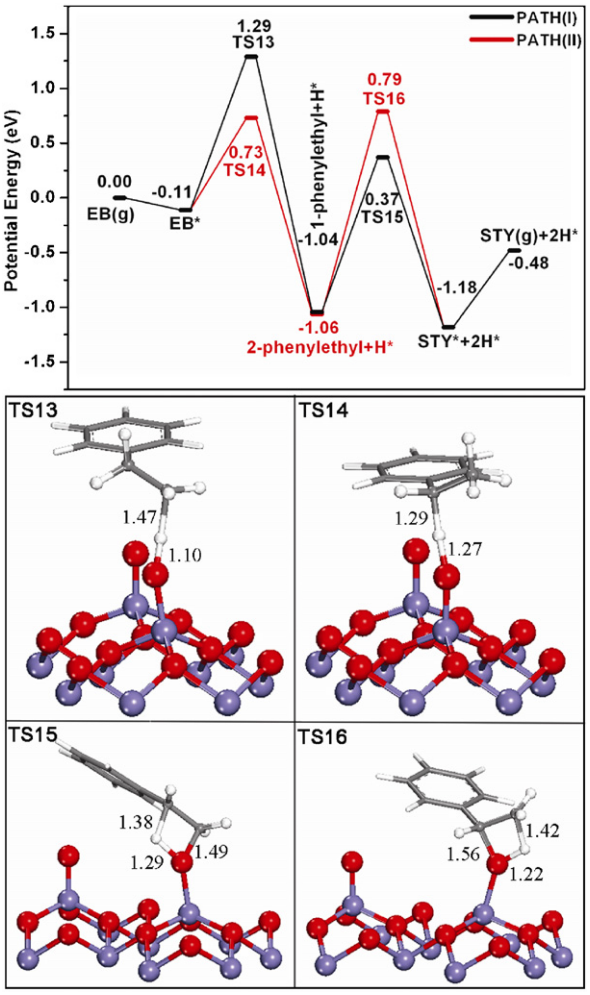

Fig. 7. Potential energy diagrams and transition states for ethylbenzene oxidative dehydrogenation on the ferryl-terminated surface.

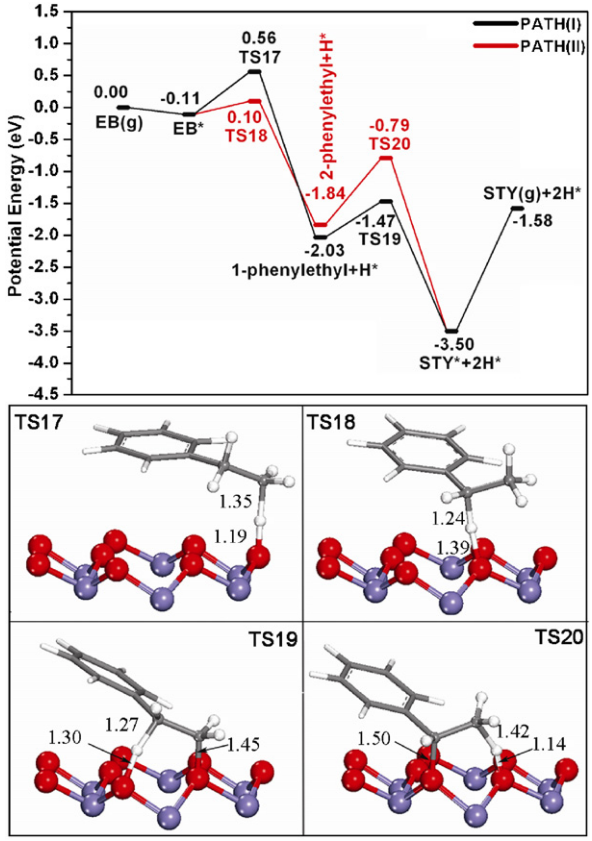

Fig. 8. Potential energy diagrams and transition states for ethylbenzene oxidative dehydrogenation on the O-terminated surface.

tion of ethylbenzene shows no preference for PATH(I) or PATH(II), arising from the nearly identical stability of the reaction intermediates. On the other hand, PATH(II) is kinetically preferred to initiate the C–H bond activation while for the detachment of the second H atom PATH(I) is more favorable. As the overall energy barriers for PATH(I) and PATH(II) are 1.29 and 0.79 eV, respectively, PATH(II) is predicted to be dominant on the ferryl-terminated surface as well.

3.3.2. H_2O formation

Over the ferryl-terminated surface, the detached H atoms will be removed in the form of H_2O. It is found that the configuration of two H atoms jointly adsorbed on the top of an O surface atom is 0.25 eV lower in energy than that where the two H atom are adsorbed separately on the top of two O surface atoms (see Fig. S23 and Table S24 in Supplementary Material). Therefore, the dehydrogenated H atoms combine with the OH species preferentially, leading to H_2O formation. Then, H_2O desorption occurs with an energy barrier of 0.91 eV, and surface O vacancies are simultaneously formed.

3.4. Oxidative dehydrogenation of ethylbenzene on the O-terminated surface

3.4.1. C–H bond activation

The O-terminated surface is another reactive surface with lattice O atoms proposed to be the active centers for dehydrogenation reactions [17,18]. The potential energy diagrams and the transition state for the oxidative dehydrogenation of ethylbenzene on the O-terminated surface are given in Fig. 8. Like the ferryl-terminated surface, the dehydrogenation reactions follow the Mars van Krevelen mechanism. All the four elementary steps are highly exothermic and release much more heat than those on the other two surfaces mentioned above. As there is a linear relationship between the activation energy for an elementary step and the reaction heat if entropy effects are neglected (the Brønsted–Evans–Polanyi relationship) [48], the energy barriers for the dehydrogenation steps drop sharply. The overall energy barriers for PATH(I) and PATH(II) are calculated to be only 0.56 and 0.10 eV. However, because of the strong binding between styrene and the O-terminated surface, the energy barrier for styrene desorption is as high as 1.92 eV. That is, the generated styrene molecules are hard to escape from the O-terminated surface and subject to the further dehydrogenation to produce byproducts. Meanwhile, it can be seen that on all the three investigated surfaces, PATH(II) is kinetically more favorable than PATH(I), i.e., the C–H activation takes place preferentially in the methylene group of ethylbenzene.

3.4.2. H_2O and H_2 formation

The removal of the generated H could be achieved via the release of H_2 or H_2O on the O-terminated surface. The energy profiles for producing H_2 and H_2O are compared in Fig. 9. In the transition state for H_2O formation (TS21), an H atom adsorbed initially at the O site reacts with an adjacent hydroxyl group to produce H_2O. The energy barrier for this elementary step is calculated to be 1.35 eV and the reaction is endothermic by 0.85 eV. Then the formed H_2O is desorbed from the surface and the corresponding energy barrier is calculated to be 1.16 eV. With the release of H_2O, the catalyst surface is reduced.

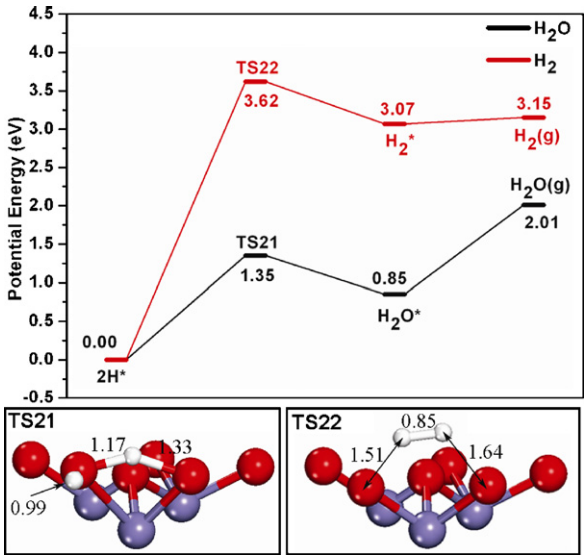

Fig. 9. Potential energy diagrams and transition states for H_2O formation and H_2 formation on the O-terminated surface.

Alternatively, two adjacent O–H bonds on the O-terminated surface are likely to be broken for the H atoms to combine. As shown in TS22 of Fig. 9, the H–O bonds are stretched to 1.51 and 1.64 Å, and simultaneously the H–H bond length is reduced to 0.85 Å. Owing to the strong H–O binding, H_2 formation is rather difficult, with a high energy barrier of 3.62 eV. Thus, it can be seen that the dehydrogenated H atoms are removed dominantly in the form of H_2O on the O-terminated surface.

3.5. Surface oxidation by CO_2

After H_2O molecules, and hence surface O vacancies, are produced, the defective ferryl- and O-terminated surfaces need to be re-oxidized to keep the reaction cycle, otherwise the catalytic activity of Fe_2O_3 would decrease dramatically with O consumption. Saito et al. [14] claimed that the lattice O atoms of metal oxides are depleted in the dehydrogenation reactions, and the reduced oxides can be recovered in the presence of CO_2; that is, CO_2 may serve as the oxidant for the catalyst recovery. On the basis of our calculated results, however, the defective ferryl-terminated surface is hard to be recovered through the oxidation of the Fe-terminated surface by CO_2 because the energy barriers for both CO_2 decomposition and the formation of HCOO are kinetically unfavorable, as compared to that for the production of COOH.

Then, the O-terminated surface with one O vacancy was used to investigate the O compensation. The adsorption energy of CO_2 at the O vacancy is calculated to be 0.45 eV (see Table S25 in Supplementary Material), with the Fe–O bond lengths of 1.89 and 2.09 Å. However, the energy barrier for CO desorption is calculated to be 2.25 eV, which is too high for CO to be released at the industrially used temperature (~870 K); that is, CO_2 cannot be used as the oxidant to compensate for the lattice O atoms on the O-terminated surface. Therefore, both the ferryl- and O-terminated surfaces are predicted to be rapidly reduced and transformed to the Fe-terminated surface after the reaction is initiated.

3.6. Dominant active surface and reaction mechanism

Comparing the energy barriers for the C–H bond activation along PATH(II) on the three surfaces (see Fig. S25 in Supplementary Material), it is apparent that the C–H bond activation on the O-terminated surface is kinetically most favored while the Fe-terminated surface is least active with the highest energy barrier. However, the energy barrier for styrene desorption is 1.92 eV on the O-terminated surface, which is too high for styrene to be released. Moreover, the adsorbed styrene may lead to deep-dehydrogenation products such as carbon deposition and aromatic, and eventually deactivate the catalyst [3]. These findings can rationalize the experimentally observed induction period which is essential before Fe_2O_3 becomes active [17]. During this period, while styrene is yielded over the O-terminated surface, the target product cannot be detected.

On the other hand, some lattice O atoms are removed with the release of H_2O on the O-terminated surface, and the Fe-terminated surface is then attained. As evidenced by the aforementioned DFT calculations, the O- and ferryl-terminated surfaces are hard to be recovered under CO_2 atmosphere, and therefore the redox cycle cannot be achieved.

When Fe^{2+} is exposed, the synergistic effect between ethylbenzene dehydrogenation and the reverse water–gas shift reaction takes place, and the coupling mechanism dominates during the steady state of the reaction, leading to the formation of H_2O and H_2. As a consequence, after H_2O is first released during the induction period, both H_2O and H_2 are predicted to be captured at the steady state, which also agrees well with the experimental observations [8]. Moreover, considering that the energy barrier for the formation of COOH is slightly lower than that for H_2 formation, the capture of the small amount of H_2 implies that both the one-step and two-step pathways contribute to the coupling mechanism although the former is dominant.

4. Conclusions

Spin-polarized DFT–GGA calculations have been performed to investigate ethylbenzene dehydrogenation in the presence of CO_2 on Fe_2O_3(0001). On the basis of the experimental information and theoretical prediction, three model surfaces with Fe-, ferryl-, and O-terminations are constructed to reveal the overall reaction mechanism and the role of CO_2 in H removal.

Then, the most stable adsorption configurations of the reactants, intermediates, and products are identified, and the transition states for the elementary steps involved have been explored using the dimer method. The calculated results indicate that on all of the three surfaces, the C–H activation in the methylene group followed by the dehydrogenation of the methyl group is kinetically more favorable. The energy barriers for ethylbenzene dehydrogenation are lowest on the O-terminated surface, and simultaneously the generated styrene is adsorbed too strongly to be released. Thus, the O-terminated surface is suggested to be the active center during the experimentally observed induction period.

With the production of styrene on the O-terminated surface, some lattice O atoms are removed through the release of H_2O, and then the Fe-terminated surface is attained. As CO_2 decomposition and the formation of HCOO ($CO_2 + 2H \rightarrow HCOO + H \rightarrow HCO + O + H \rightarrow HCO + OH$) are hindered by the relatively high activation energies, CO_2 cannot serve as the oxidant to recover the O- and ferryl-terminated surfaces to keep the redox cycle.

At the steady state of the reaction, the coupling mechanism dominates on the Fe-terminated surface. With the synergistic effect between ethylbenzene dehydrogenation and the reverse water–gas shift reaction through the formation of COOH, both H_2O and H_2 are produced. Since the energy barrier for the formation of COOH ($CO_2 + 2H \rightarrow COOH + H \rightarrow CO + OH + H \rightarrow CO + H_2O$) is comparable to that for H_2 formation, both the one-step and two-step pathways are predicted to contribute to the coupling mechanism, although the former is more probable.

Acknowledgements

This research is supported by Science and Technology Innovation Foundation of China National Petroleum Corporation (No. 2008D-5006-05-05), Natural Science Foundation of China (Nos. 21003046, 20736011), Doctoral Fund of Ministry of Education of China (No. 200802511007), and Fundamental Research Funds for Central Universities (No. WA1014027). The computational time provided by Notur project is highly acknowledged (nn4685k).

Appendix A. Supplementary data

Supplementary data associated with this article can be found, in the online version, at doi:10.1016/j.molcata.2011.05.002.

References

[1] Z.F. Qin, J.G. Liu, A.L. Sun, J.G. Wang, Ind. Eng. Chem. Res. 42 (2003) 1329–1333.
[2] M. Sugino, H. Shimada, T. Turuda, H. Miura, N. Ikenaga, T. Suzuki, Appl. Catal. A 121 (1995) 125–137.
[3] S. Chen, Z. Qin, A. Sun, J. Wang, J. Nat. Gas Chem. 15 (2006) 11–20.
[4] A. Sun, Z. Qin, J. Wang, Appl. Catal. A 234 (2002) 179–189.
[5] N. Mimura, M. Saito, Catal. Lett. 58 (1999) 59–62.
[6] N. Mimura, M. Saito, Catal. Today 55 (2000) 173–178.
[7] T. Badstube, H. Papp, P. Kustrowski, R. Dziembaj, Catal. Lett. 55 (1998) 169–172.
[8] J.S. Chang, S.E. Park, M.S. Park, Chem. Lett. 26 (1997) 1123–1124.
[9] A.L. Sun, Z.F. Qin, S.W. Chen, J.G. Wang, J. Mol. Catal. A 210 (2004) 189–195.
[10] W.P. Addiego, W. Liu, T. Boger, Catal. Today 69 (2001) 25–31.
[11] N. Dulamita, A. Maicaneanu, D.C. Sayle, M. Stanca, R. Craciun, M. Olea, C. Afloroaei, A. Fodor, Appl. Catal. A 287 (2005) 9–18.
[12] N. Mimura, I. Takahara, M. Saito, T. Hattori, K. Ohkuma, M. Ando, Catal. Today 45 (1998) 61–64.
[13] W.P. Addiego, C.A. Estrada, D.W. Goodman, M.P. Rosynek, J. Catal. 146 (1994) 407–414.
[14] K. Saito, K. Okuda, N. Ikenaga, T. Miyake, T. Suzuki, J. Phys. Chem. A 114 (2010) 3845–3854.
[15] T. Badstube, H. Papp, R. Dziembaj, P. Kustrowski, Appl. Catal. A 204 (2000) 153–165.
[16] X.M. Zhu, M. Schon, U. Bartmann, A.C. van Veen, A. Muhler, Appl. Catal. A 266 (2004) 99–108.
[17] C. Kuhrs, Y. Arita, W. Weiss, W. Ranke, R. Schlögl, Top. Catal. 14 (2001) 111–123.
[18] W. Weiss, D. Zscherpel, R. Schlögl, Catal. Lett. 52 (1998) 215–220.
[19] W. Weiss, W. Ranke, Prog. Surf. Sci. 70 (2002) 1–151.
[20] W. Weiss, R. Schlögl, Top. Catal. 13 (2000) 75–90.
[21] G. Kresse, J. Hafner, Phys. Rev. B 48 (1993) 13115–13118.
[22] G. Kresse, J. Furthmüller, Comput. Mater. Sci. 6 (1996) 15–50.
[23] G. Kresse, J. Furthmüller, Phys. Rev. B 54 (1996) 11169–11186.
[24] J.P. Perdew, K. Burke, M. Ernzerhof, Phys. Rev. Lett. 77 (1996) 3865–3868.
[25] P.E. Blöchl, Phys. Rev. B 50 (1994) 17953–17979.
[26] D. Sheppard, R. Terrell, G. Henkelman, J. Chem. Phys. 128 (2008) 134106.
[27] W. Bergermayer, H. Schweiger, E. Wimmer, Phys. Rev. B 69 (2004) 195409.
[28] T. Schedel-Niedrig, W. Weiss, R. Schlögl, Phys. Rev. B 52 (1995) 17449–17460.
[29] G. Rollmann, P. Entel, A. Rohrbach, J. Hafner, Phase Transitions 78 (2005) 251–258.
[30] G. Rollmann, A. Rohrbach, P. Entel, J. Hafner, Phys. Rev. B 69 (2004) 165107.
[31] F. Alvarez-Ramirez, J.M. Martinez-Magadan, J.R.B. Gomes, F. Illas, Surf. Sci. 558 (2004) 4–14.
[32] X.G. Wang, W. Weiss, S.K. Shaikhutdinov, M. Ritter, M. Petersen, F. Wagner, R. Schlögl, M. Scheffler, Phys. Rev. Lett. 81 (1998) 1038–1041.
[33] A. Rohrbach, J. Hafner, G. Kresse, Phys. Rev. B 70 (2004) 125426.
[34] S. Thevuthasan, Y.J. Kim, S.I. Yi, S.A. Chambers, J. Morais, R. Denecke, C.S. Fadley, P. Liu, T. Kendelewicz, G.E. Brown, Surf. Sci. 425 (1999) 276–286.
[35] M.E. Greene, A.N. Chiaramonti, S.T. Christensen, L.X. Cao, M.J. Bedzyk, M.C. Hersam, Adv. Mater. 17 (2005) 1765–1768.
[36] S.A. Chambers, S.I. Yi, Surf. Sci. 439 (1999) 785–791.
[37] C. Lemire, S. Bertarione, A. Zecchina, D. Scarano, A. Chaka, S. Shaikhutdinov, H.J. Freund, Phys. Rev. Lett. 94 (2005) 166101.
[38] X.Y. Ma, L. Liu, J.J. Jin, P.C. Stair, D.E. Ellis, Surf. Sci. 600 (2006) 2874–2885.
[39] S.X. Yin, X.Y. Ma, D.E. Ellis, Surf. Sci. 601 (2007) 2426–2437.
[40] G. Henkelman, H. Jonsson, J. Chem. Phys. 111 (1999) 7010–7022.
[41] S.K. Shaikhutdinov, Y. Joseph, C. Kuhrs, W. Ranke, W. Weiss, Faraday Discuss 114 (1999) 363–380.
[42] S. Chen, Z. Qin, X. Xu, J. Wang, Appl. Catal. A 302 (2006) 185–192.
[43] W.X. Huang, W. Ranke, R. Schlögl, J. Phys. Chem. B 109 (2005) 9202–9204.
[44] W.X. Huang, W. Ranke, R. Schlögl, J. Phys. Chem. C 111 (2007) 2198–2204.
[45] A.C. Dupuis, M. Abu Haija, B. Richter, H. Kuhlenbeck, H.J. Freund, Surf. Sci 539 (2003) 99–112.
[46] B. Dillmann, F. Rohr, O. Seiferth, G. Klivenyi, M. Bender, K. Homann, I.N. Yakovkin, D. Ehrlich, M. Baumer, H. Kuhlenbeck, H.-J. Freund, Faraday Discuss 105 (1996) 295–315.
[47] P. Mars, D.W. van Krevelen, Chem. Eng. Sci 3 (1954) 41–59.
[48] M. Boudart, in: G. Ertl, H. Knözinger, J. weitkamp (Eds.), Handbook of Heterogeneous Catalysis, Wiley-VCH, Inc, Weinheim, 1997, p. 1.